

Kirigami-enabled, Passive Resonant Sensors for Wireless Deformation

Monitoring

Sadaf Charkhabi¹, Yee Jher Chan¹, Doh-Gyu Hwang², Sean T. Frey², Michael D. Bartlett^{*2}, and Nigel F. Reuel^{*1}

* reuel@iastate.edu for resonant sensors and applications

* mbartlet@iastate.edu for kirigami-enabled soft materials

1. Department of Chemical and Biological Engineering. Iowa State University

2. Department of Material Science and Engineering. Soft Materials and Structures Lab. Iowa State University

Abstract

A passive resonant sensor with kirigami patterning was used to wirelessly report material deformation in closed systems. The sensors were fabricated from copper-coated polyimide by etching a conductive Archimedean spiral which was then laser cut to add kirigami-inspired patterns. The sensor response was defined as the resonant frequency in the transmission scattering parameter signal (S_{21}), which was captured via a two-loop reader antenna and a benchtop vector network analyzer (VNA). The sensors were tested over a 0-22 cm range of extension and showed a significant shift in resonant frequency (e.g. 90 MHz shift for 10 cm stretch of the resonator with 3 mm pitch size). Furthermore, the effect of resonator coil pitch on the extension sensor gain (MHz/cm) and linear span of the sensor was studied. The repeatability of the sensor gain was confirmed by performing three extension hysteresis cycle

experiments and the gain showed a linear increase with pitch size and low variability (linear model with $R^2 = 0.99$). The 5 mm pitch sensor was coated with 0.5, 1, and 2 mm thick polydimethylsiloxane (PDMS) films to protect from electrical shorting in aqueous environments. The extensional sensor gain of the coated resonator was found to vary linearly with the coating thickness. The coated resonators were placed in a PVC pipe to report flow rates. As film thickness increased, we observed an increasing breakthrough volumetric flow rate before the sensor responded, after which a linear flow sensor gain is observed. Of the three tested, the sensor with 1 mm coating was found to have the largest gain (0.17 MHz·s/mL) and linear span (10-100 ml/s). Thus, flexible resonant sensors with kirigami-inspired patterns can be tuned via geometric and coating considerations to wirelessly report a large range of extension lengths for potential uses in health monitoring, motion tracking, deformation detection, and soft robotics.

1. Introduction

Position and deformation sensing are critical for applications ranging from virtual reality and robotics to motion tracking and health monitoring.^[1–4] These sensors can be used to provide positional feedback for actuator systems,^[5,6] estimate the pose and configuration of mechanical or human systems,^[7–9] and determine the deformation of a material or structure.^[10–12] Recent emphasis on un-tethered systems requires light, compact, and energy-efficient deformation sensors.^[13] Additionally, implementation into wearable sensors for human monitoring and soft robotics systems demand significant extents of deformation.^[14–20] Furthermore, wireless monitoring in these systems can reduce system complexity by eliminating or reducing wiring components and can enable more compliant materials by removing semi-rigid wiring and connection points.^[21,22] Thus, wireless monitoring of deformation with passive elements can provide a path forward for deformation sensing in soft bodies for energy-efficient reporting and control.^[23]

Wired soft sensors can provide a solution when integrated with wireless communication circuitry (Wi-Fi, Bluetooth, or cellular).^[24] These include various designs of stretchable strain sensors, such as dipole, serpentine, spiral, and helical geometries composed of strain-dependent resistive elements such as carbon impregnated rubbers or compliant microfluidic channels filled with liquid metals.^[25–27] In each of these cases, the extra wiring and power consumption of the communication circuitry can limit the utility of un-tethered applications. Progress is being made on integrating more flexible, wireless sensors for feedback and control of un-tethered systems. A common solution is imaging, in which motion and position of the device are monitored externally by a camera.^[28,29] This works well in structured environments;

1 however, in unstructured environments, where a camera may be blocked or unavailable, this
2 can be a significant challenge. Another approach is the use of resonant sensors to wirelessly
3 report a positional change of soft materials.

4 Resonant sensors are a long-standing class of passive, wireless sensors that use radio frequency
5 electromagnetic radiation to wirelessly interrogate the scattering parameters of an inductor-
6 capacitor-resistor (LCR) circuit.^[30] The resonant circuit responds to changes in the local
7 dielectric (changes circuit capacitance) which has been exploited for measuring physical
8 parameters such as fluid level, pressures, temperature, and biocatalyst activity.^[31–39] Flexible
9 LCR sensors have been used to wirelessly measure the strain of compliant materials, such as
10 inductors composed of serpentine copper traces formed as planar^[40] or helical coils.^[41] In the
11 case of the planar coils, the force is set coplanar to the resonator, and the response is
12 predominantly caused by a change in the self-capacitance^[42] (C) of the LCR circuit. In the case
13 of a helical coil, the force is set normal to the spiral plane, the helical distributed length
14 changes, causing a change in inductance (L) which dominates the response. In both cases, the
15 strain causes a geometric change, which causes the resonant frequency of the LCR to shift,
16 however, due to the design of these sensors, they can only report strains of 0 to 0.3, or in the
17 case of the ~3cm structures, a deformation of up to 1cm. Stretchable antennas can also be used
18 to measure deformation; these are primarily based on liquid metals, but recent works have also
19 shown strategies for metallic deformable antennas.^[43] However, most examples require
20 connected equipment to transmit data, which limits deployment and deformation tracking in
21 dynamic systems.^[44–46] Recently, an elastomer based-liquid metal wireless strain sensor
22 measured deformations up to 50% strain in the radio-frequency range.^[47]

Emerging techniques in origami and kirigami engineering offer opportunities to create highly tunable materials and interfaces with complex three-dimensional structures, high extensibility, and tunable stiffness.^[48–54] Kirigami is the artistic cousin of origami, in which material is cut (rather than folded) to control structure. In terms of strain or deformation monitoring, most kirigami approaches have used resistive or capacitive measurements, requiring a tethered connection,^[55–57] or have used tethered antennas.^[58] Wireless kirigami and origami antennas have been demonstrated where the resonant frequency can be tuned based on the extent of folding or deformation.^[59–61] However, these demonstrations stop short of exploiting such structures to report the extension length via the resonant scattering parameters of the kirigami antenna. Moreover, these are fabricated to have resonant frequencies suitable for telecommunication (GHz) and not lower frequencies for penetration through water and other biologic media (kHz-MHz range).^[62,63]

Herein we present a passive resonant sensor that can be engineered into an extensional sensor with a specific gain and dynamic range based on the pattern of kirigami cuts. The kirigami approach allows this new class of LCR sensors to report much larger deformations normal to their surface ($>10\times$ sensor thickness) than previous, encapsulated helical structures.^[41] In this work, planar Archimedean copper traces are patterned on a flexible substrate and cut to allow deformation normal to the planar surface, thus exploiting both changes in inductance and self-capacitance. Moreover, we show how the resonator can be coated to protect from an aqueous environment and the effect these coatings have on the sensor gain and dynamic range. Finally, we demonstrate the extensional sensor in a closed system, in this case monitoring the volumetric flow rate of water in a closed pipe (a wireless deflection vane).

2. Results and Discussion

Resonators with fixed outer and inner diameters and varying coil pitch sizes (Fig 1a) were fabricated (Fig 1b) from etched copper-coated polyimide (Pyrallux®) as reported before with the additional steps of coating the resonator with a hydrophobic polymer and laser cutting to release the kirigami coil (see Experimental section).^[39] Pitch (P) is defined as the spacing between the inductive coil lines and the cut is made in the center of the lines (at $P/2$). These resonators were interrogated by stretching vertically in a 24 cm distance between two reader antenna loops (Fig 1c,1d, and Fig S1) which were connected to a benchtop vector network analyzer (VNA). For each sensor, the magnitude of the transmission signal (S_{21}) was monitored over a frequency range of 1-300MHz (Code S2). By comparing the resonator's S_{21} magnitude from the rest position to an extended state, it was observed that stretching the sensor causes a significant change in the S_{21} response (Fig 1e). This is attributed to a change in the coil's self-capacitance and inductance that is observable in the read range of the interrogating antenna, as described below. The S_{21} response was simplified by tracking the resonant frequency defined as the minimum of the sigmoidal S_{21} feature (160 and 250 MHz in Fig 1e) (Code S3), as done in other LCR works.^[40]

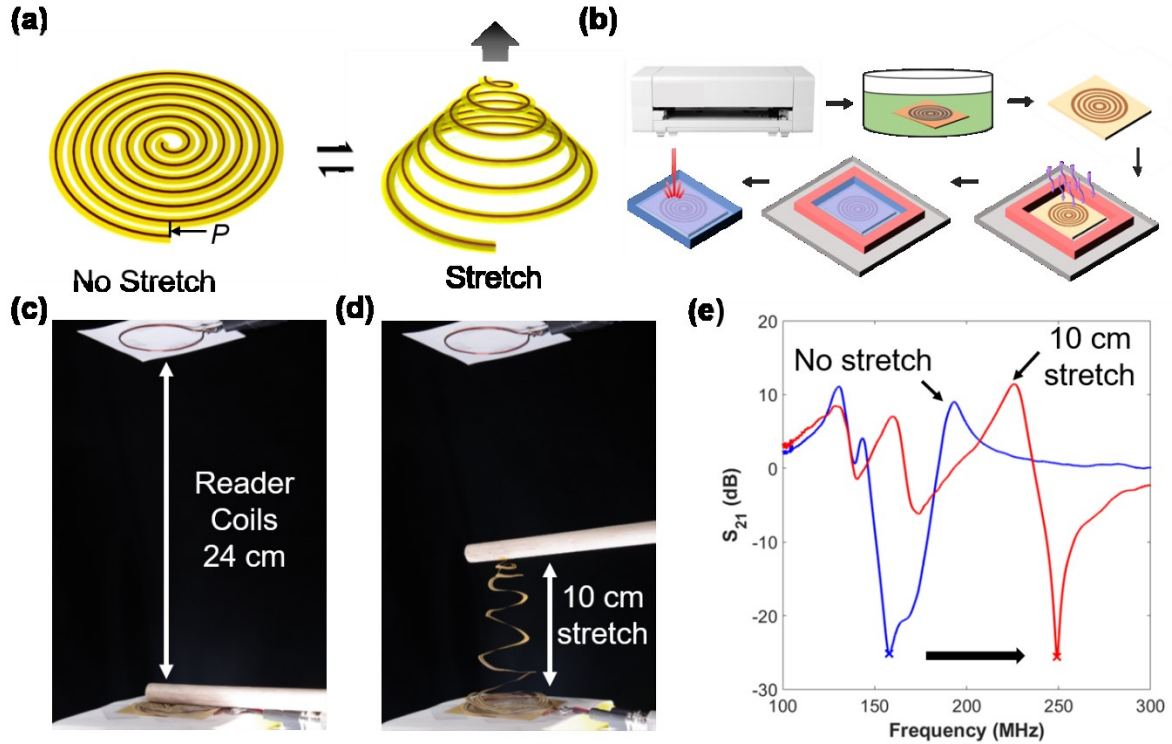


Figure 1 – a) Design of a kirigami deformation sensor based on an Archimedean spiral at rest and extended; the pitch (P) is the spacing between the resonant traces. b) The fabrication process of the kirigami resonator which includes patterning the resonator trace, etching, releasing mask, coating, and laser cutting. c) The vertical extension test setup with a 3 mm pitch, 5 mm inner diameter, and 54 mm outer diameter resonator at rest (no extension) and d) with 10 cm extension. e) The S_{21} magnitude response from the sensor in (c) and (d) depicting the signal minimum used to specify the resonant frequency (marked with 'x').

The kirigami resonant sensor response was observed over a wide range of stretch distances (0-22 cm at 1 cm intervals) to determine the linearity of sensor response. A linear increase in the resonant frequency was observed as the sensor was stretched (Fig 2) up to a specified length; then the resonant frequency sharply remained constant. The proposed mechanism of this response is a change in both the circuit self-capacitance and inductance. When the kirigami

LCR resonator is at rest, the self-capacitance is dictated by the coil to coil spacing.^[42] When the resonator is pulled out of plane this spacing is increased, and the capacitance decreases much like the spacing of a parallel plate capacitor (Eq. 1) where C is the capacitance, ϵ_0 is the permittivity of free space ($8.854 \cdot 10^{-12}$ F/m), ϵ_r is the relative permittivity of the material, A is the capacitive area, and d is the capacitor plate displacement.^[64] Additionally, when the resonator with N number of turns is pulled out of plane it resembles a helical coil, where the inductance (L) is defined by (Eq. 2) in which K is the correction factor, l is the axial distributed length, A is the cross-sectional area, and μ_r and μ_0 represent the relative permeability and the permeability of free space, respectively. Thus as the resonator is extended, the length of the coil increases, and the inductance decreases. Since the resonant frequency has an inverse relationship with the capacitance and inductance (Eq. 3 where L is the inductance and C is the capacitance)^[65], the resonant frequency would increase by extending the resonant sensor. We observe the sharp leveling off of the sensor response (Fig 2b) at the point where all the resonator rings have been lifted off the surface near the interrogating reader antenna. In all geometries tested the sensor will continue to extend, but the coils begin to warp and the sensor begins to approach a more linear wire geometry, as described below.

$$C = \frac{\epsilon_0 \epsilon_r A}{d} \quad (\text{Eq. 1})$$

$$L = K \mu_r \mu_0 \frac{N^2 A}{l} \quad (\text{Eq. 2})$$

$$\text{Resonant Frequency} = \frac{1}{2\pi\sqrt{LC}} \quad (\text{Eq. 3})$$

1 This extension test was repeated for kirigami resonators with different pitches of 3, 4, and 5
2 mm (Fig 2b). In order to study the effect of the resonator's geometry, we characterize two
3 parameters i) the sensor gain, defined as the linear slope of the frequency versus stretch curve,
4 and ii) the sensor span, defined as the maximum linear deformation the kirigami resonant
5 sensor can report. The gain and span were both found to vary as a function of the resonator
6 pitch. Again, the plateau of the resonant frequency (sensor span) is attributed to the warping
7 and twisting of the kirigami resonant sensor out of the plane of the readers after a certain
8 stretch distance (Video S4). At this threshold, an increase in extension causes the sensor to
9 twist and elongate, changing from a parallel helical coil to an extended wire perpendicular to
10 the reader loops. This change in deformation pattern, from increasing the coil-coil spacing and
11 helical coil distributed length to a change in perpendicular wire length, would describe this
12 phenomenon. The aforementioned change in capacitance and inductance would no longer be
13 dominant during the wire extension phase and the resonant frequency would remain constant.
14 At this point, the circuit begins to approximate a linear antenna, where the resonant frequency
15 is dictated by the length of conductor alone. The sensor span decreases as the pitch size
16 increases. This observation is attributed to the length of the resonator; a smaller pitch
17 corresponds to an LC sensor with larger length (Table S5). A longer resonator length allows for
18 the coils to stay co-planar for a longer extension length, thus increasing the span of the sensor,
19 however, this also reduces the sensor gain.

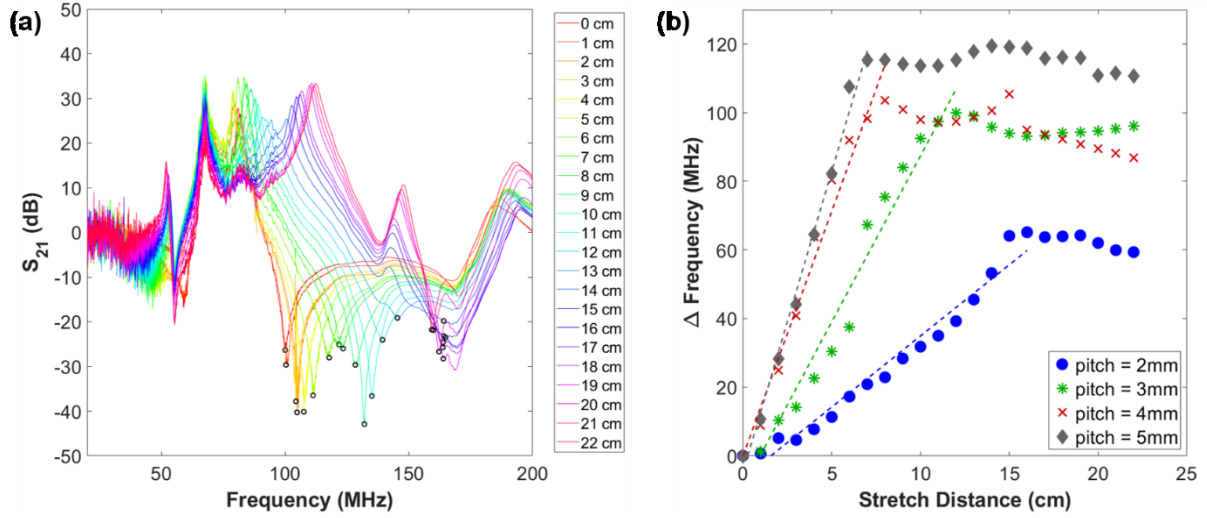


Figure 2 – a) Kirigami resonant sensor response found from the minima of resonant frequency peaks (circle points) in the transmission magnitude (S_{21} (dB)) response, scanned over the 0-200 MHz frequency range; data shown here for the 2 mm pitch sensor extended from 0-22 cm. b) Resonant frequency response to different stretch distances for kirigami resonators with varying pitch sizes.

To check the reversibility of the sensors, we performed hysteresis experiments in which each sensor was stretched and released three times and the gains were calculated during extension and relaxation (Fig 3a). The extent to which the sensor was stretched was modified based on the pitch size to make sure that the response remains in the linear portion of the frequency response (*i.e.* within the sensor span). Each sensor geometry exhibited a small standard deviation of the gain (Fig 3b). Also, the gain increases linearly with the pitch size of the resonator (equation insert in Fig 3b). As the pitch size increases, the length of the resonator spiral decreases and thus a larger amount of the spiral is pulled out of the interrogation range of the bottom reader coil when extended (Fig S6), thus causing a more dramatic shift in resonant frequency. The linear model fit to the gain versus pitch data has a high coefficient of

1 determination (R^2) at 0.99, thus demonstrating the ability to choose sensor gain based on
2 kirigami resonator pitch size. Moreover, we cycled the 5 mm pitch resonator to 96 cycles to
3 approximate a sensor that undergoes repetitive extensions (Fig S7). In this case we found the
4 sensor gain to remain constant, at 14.17 ± 0.20 , 14.12 ± 0.10 , 14.24 ± 0.14 MHz/cm, for 1-10,
5 51-53, and 94-96 cycles respectively (95% confidence intervals).

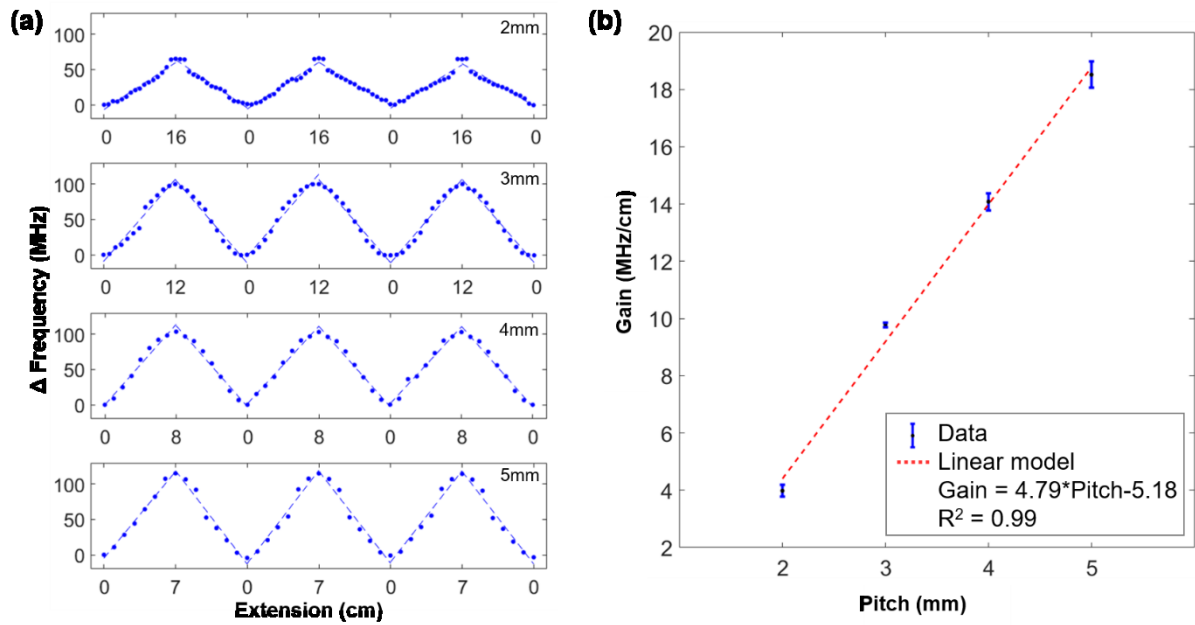


Figure 3 – a) Kirigami resonant sensor response in a three-cycle hysteresis experiment to
determine the consistency of sensor gain (dashed line fit) for different sensor pitch sizes. b)
Gains reported for different pitch sizes and the model (dotted line) showing a linear dependence
of gain on pitch size. Error bars refer to one standard deviation for $n=6$ gains.

The next step to embedding these sensors in actual systems is to protect the conductive surface
from shorting, especially in water-based applications. Thus, the sensors were coated with
polydimethylsiloxane (PDMS) to insulate the LCR resonator from the external environment. For
this purpose, the resonator with $P = 5$ mm was chosen as the test candidate since it has the

1 steepest gain (*e.g.* most responsive). The resonators were coated with varying thicknesses (0.5,
2 1, and 2 mm cast height, actual height after curing reported in methods) of PDMS by casting the
3 elastomer on the sensor placed within a defined mold. To determine the effect of coating
4 thickness on the sensor gain, three extension hysteresis cycle tests were performed on each
5 resonator in air and the changes in the resonant frequency were measured (Fig 4a). The sensor
6 gain was calculated based on each extension and retraction trend (six times in total for each
7 sensor) and was compared for different coating thickness (Fig 4b). The maximum extension was
8 kept constant at 7 cm for each sensor.

9 We first observed that starting resonant frequencies were lower for all coated sensors, which
10 we attribute to the altered dielectric environment. The relative permittivity for air and PDMS is
11 1 and 2.5 respectively at room temperature which results in a different frequency response
12 window (Fig S8). Next, we observed a seemingly discontinuous trend in sensor gain as the
13 coating thickness increases (Fig 4b). The uncoated sensor exhibits the highest gain, the
14 minimally coated sensor (0.5mm) gain is essentially halved, and then the sensor gains increase
15 as the coating thickness is increased. As described above the sensor response is attributed to
16 geometric changes, but in this case, the coil geometry is the same between all sensors; thus the
17 coating must also have an effect on the manner in which the coil unfolds and extends. Upon
18 closer inspection of stretching footage (Fig S9), we observe that the uncoated coil has very little
19 mass and the polyimide substrate is sufficiently rigid to maintain a regular, helical coil structure.
20 However, the minimal coating adds mass to the coil and due to the large coil compliance, less of
21 the coil length extends from the surface. As the encapsulant coating increases, the coil rigidity
22 increases more rapidly than the added mass and the coil deforms in a manner more similar to

1 the uncoated helical coil. Additionally, we observe an increased variance in the coated
 2 resonator gains as compared to the uncoated resonators. This is likely due to the
 3 inconsistencies caused by PDMS coating such as stochastic stick-slip phenomena as the PDMS
 4 layers rub against each other during extension which could be reduced in the future be
 5 increasing the cut width.

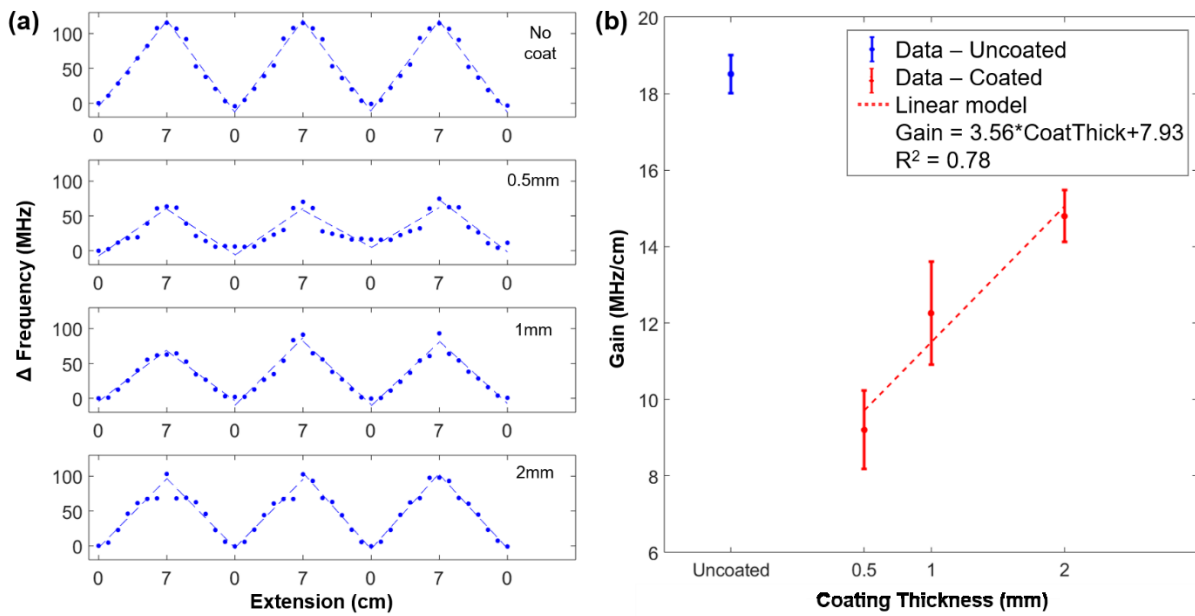


Figure 4 – a) PDMS-coated, kirigami resonant sensor response to three hysteresis cycles at 0, 0.5, 1, and 2 mm cast thicknesses of PDMS on a 5 mm pitch sensor showing consistent gains in air (dashed line fit). b) Measured gains for the coated sensors with error bars showing one standard deviation for $n=6$ gains. Linear model (dashed line) shows a linear relation of gain to coating thickness for 0.5 to 2mm coating thickness.

To determine the applicability of these sensors in a closed system, we utilize PDMS coated resonant sensors to wirelessly measure the flow rate of liquid in a closed pipe. The sensor was placed in a 6 cm diameter PVC pipe (transparent for visual confirmation of extension) oriented

1 vertically (such that gravity pulls down on the sensor) and we measured the effect of flow rate
2 on sensor response (Fig 5a). The response was observed using two reader antennas looped
3 externally around the pipe at a displacement of 10 cm and connected to the VNA. The center of
4 the resonator was fixed parallel to the top reader loop while the rest of the coil was free to
5 extend or retract with the water flow. The pipe was initially filled with water and flow rates in
6 the range of 0-100 mL/s were added via a manual control valve.

7 As anticipated, increasing the water flow rate increased the resonator's extension length which
8 subsequently increased the resonant frequency. A thicker PDMS coating results in a higher
9 sensor stiffness and decreases the extent to which the kirigami resonator stretches for a given
10 flow rate (Fig 5b and Video S10). The change in resonant frequency as a function of flow rate
11 was also recorded for different coating thicknesses (Fig 5c). The range of frequency shifts is
12 significantly lower in water when compared to the same resonator in air. We attribute this to
13 the dielectric effect of water ($\epsilon_r \approx 80$ at 20°C) which shifts the resonant frequency from 240-370
14 MHz to 85-100 MHz (Fig S11). The resonant frequency is dominated by this water effect and
15 thus the effect of extension is less pronounced on these submerged sensors. Also, in the pipe,
16 the kirigami resonator at no flow rate is not flat (as it is in the resting condition measured in air)
17 thus the effect of extension due to flow rate would again be less than that observed in air.

18

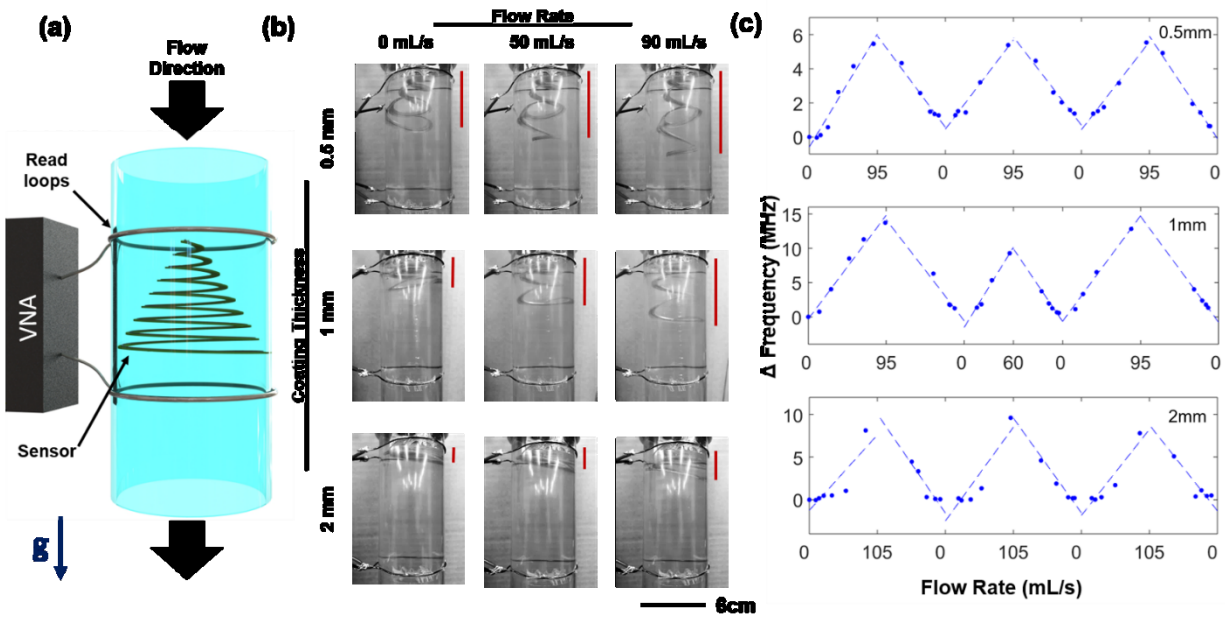


Figure 5 – a) Schematic of a kirigami resonant sensor reporting the flow rate of water in a closed pipe. b) Images of the sensor stretching caused by water flow through a clear pipe (supplement videos also provided in S8). c) Three cycle hysteresis experiment to observe changes in the resonant frequency based on the flow rate and dependence on coating thickness. Linear gain model shown with dashed lines.

From the hysteresis plots of the kirigami resonant sensors in a flowing pipe (Fig 5c), we observe that the flow sensor gain (change in frequency response divided by the change in flow rate) was not linear with flow rate (as was observed with uniaxial extension). In Fig 6, all the data is presented together, and we clearly observe a threshold flow rate (Q_{BT}) before a linear response is again observed. We attribute the breakthrough flow rate to either the friction between adjacent coils caused by the coating or a non-linear, force-displacement response of the kirigami. This threshold flow rate increases as the coating thickness increases. A higher variation in the gain was observed for thicker coatings, attributed to the stick-slip

phenomenon as before. Thicker coatings increase the gain, but if too much is added, it increases the requisite breakthrough flow rate, which would not allow for reporting lower flow rates. From this panel of sensors, the 1 mm coated is optimal since its gain is relatively high and the Q_{BT} is low; however, for a system with low flow rates (below 10 mL/s), the 0.5 mm coating is suggested since it has no observed breakthrough flow rate. The breakthrough limit is not observed in the preceding air extension experiments as those were conducted at specified extension lengths and do not indicate the force required to reach that extension.

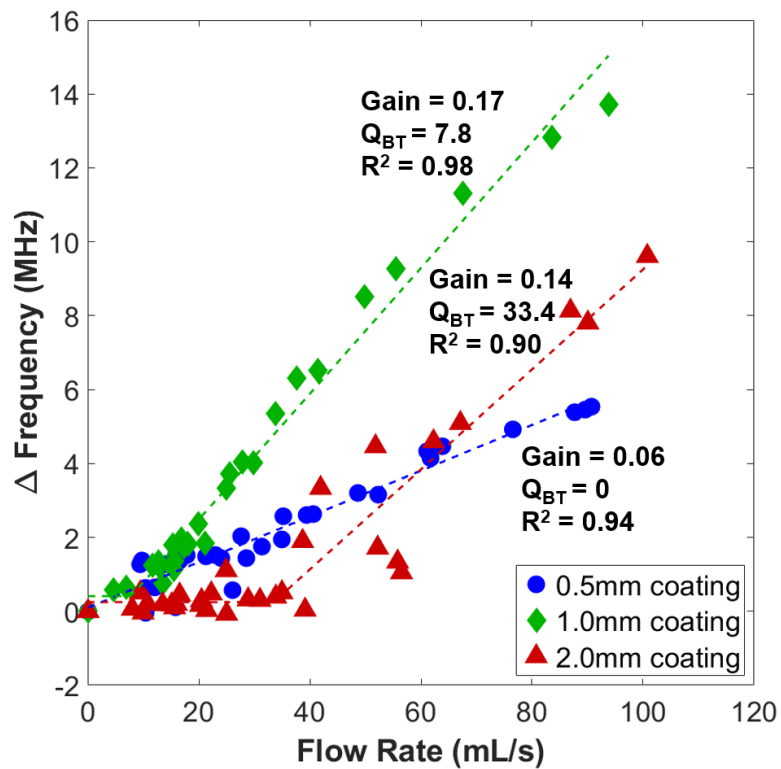


Figure 6 – The effect of water flow rate on the changes in resonant frequency for 5 mm pitch resonators with 0.5, 1, and 2 mm cast thickness of PDMS coating affixed in a 6 cm diameter pipe. The data were fit with a linear gain with an additional parameter of a breakthrough flow rate. Reported flow sensor gains, breakthrough flow rate, and model coefficient of

determination for each coating thickness are presented on the plot. The units for gain and Q_{BT} are MHz·s/ml and ml/s, respectively.

3. Conclusion

Here we demonstrate the design, fabrication, characterization, and application of kirigami resonant sensors for wireless reporting of extension and retraction in closed environments. The sensor response was monitored wirelessly using a vector network analyzer, observing the changes in resonant frequency in the transmission scattering parameter magnitude (S_{21}). Unlike many previously reported resonant deformation sensors which usually work in mm extension ranges, the linearity of this kirigami-inspired resonant sensor can be as high as 16cm. Furthermore, it was shown that by coating the resonator with PDMS film, the sensor can be applied in both air and aqueous systems. This was demonstrated by wirelessly measuring the flow rate of water in a closed piping system. The kirigami resonator gain exhibits low variability in hysteresis experiments and can be controlled based on pitch size and coating thickness. This portends to their use as reliable and tunable sensors. We anticipate that this type of deformation sensor can be utilized in a variety of applications such as wearable bio-monitoring and untethered robotics, where low power, wireless sensing combined with high extensibility can enable monitoring and control of future untethered systems.

4. Experimental Section

Fabrication of resonator for stretching test: A Circular Archimedean spiral was selected as the pattern for the resonant sensors as it is common, well-characterized in literature,^[66] and has a

geometry applicable for our intended closed system application (pipe with round cross-section). Archimedean spiral resonant traces having an inner diameter of 2 mm, an outer diameter of 54 mm, and varying pitch sizes in the range of 2-5 mm were designed using Rhino 5 software (Fig 1a). The main reason for choosing the above-mentioned dimensions was to keep the resonant frequency of the coated and embedded kirigami sensors below the microwave frequency to achieve a larger penetration depth in water. The cut trace was patterned as a spiral shape having the same pitch size as the resonator and the inner diameter was modified so that the cut trace would be in the middle of the resonator trace. The resonator trace was patterned on Pyralux sheet, which is a thin copper layer (35 μm) on polyimide (25 μm), using an X-Y Plotter and an indelible marker (Fig 1b). The Pyralux was then etched in order to remove the unmasked copper using a traditional etchant solution consisting of the 2-1 volumetric ratio of hydrogen peroxide (H_2O_2) and hydrochloric acid (HCl). As the final step for the resonator preparation, the samples were washed with acetone to release the mask. The cut pattern was then created on the resonator sample using a CO_2 laser cutter so that an onion ring-shaped kirigami-based resonant sensor was fabricated.

Stretching test measurement: The kirigami sensor was wirelessly coupled with a reader antenna consisted of two copper loops having a similar diameter of 54 mm and positioned facing towards each other at a 24 cm distance. The reader antenna was connected to a vector network analyzer (VNA) for monitoring the scattering parameters matrix (S-parameters) of the sensor by capturing the phase and the magnitude of the forward transmission (S_{21}) response between 100-500 MHz. A measurement without sensor was first taken to serve as a control data, where the subsequent data will be subtracted by this data. The sensor was placed at one

end of the copper loop and the center of the sensor was taped to a wooden stick. The sensor was stretched by moving the wooden stick towards the other copper loop. The measurement was taken for every 1 cm movement of the wooden stick until it reached the copper loop at the other end. Then, measurement was taken for every 1 cm of the wooden stick moving backward to its original position. This cyclic experiment was repeated for three times.

Fabrication of coated resonators: Spiral resonant traces with no inner diameter and an outer diameter of 42.5 mm were used to fit inside the pipe. The traces were etched using the same approach as described above. After etching, the sensor was placed on an acrylic plate within a mold of a set casting thicknesses (0.5, 1.0, and 2.0 mm) and then subjected to oxygen plasma treatment at medium power and 750 mTorr for 5 min to improve bonding application (PDC-001; Harrick Plasma). A batch of PDMS elastomer (Sylgard 184 with a 10:1 oligomer-to-curing agent ratio; Dow Corning) was cast in the mold and cured at 80°C for 4h. The heights of the cured films were measured in five places and found to have final heights of 0.47 (± 0.1), 0.74 (± 0.11), and 1.63 (± 0.92) mm (95% confidence intervals). The sealed sample was then laser machined (Epilog Laser Fusion M2, 75 watts) in the spiral pattern.

Resonator response measurements under a flowing system: In this experimental setup, the two copper wire loops were wrapped around a transparent PVC pipe having an inner diameter of 5.08 cm, an outer diameter of 6.03 cm, and a length of 30.5 cm. The distance between the copper loops was 10 cm. With the pipe positioned vertically, the center of the sensor is fixed at the same height as the upper copper loop. A minimal cross-shaped structure made by cellophane tape was connected to the center of the sensor and adhered to the pipe wall. This structure helps to fix the sensor in the middle of the pipe. Fittings were attached to both ends

of the pipe and connected to two tubes: (1) a water supply tube at top and (2) drain tube at the bottom. As the direction of water flow in the pipe is proportional to gravity, the system was first filled with water prior to initializing a flow rate to prevent the presence of air gap within the system. The water flow rate was then tuned by controlling the globe valve of water supply. The water flow rate was determined by measuring the amount of time for the water outlet flow to fill up a 500 mL measuring cylinder. Same VNA device as above was used to read the transmission response (10-500 MHz) for every flow rate tuned. The experiment was started with a small flow rate, slowly increased, then decreased, for three cycles, where 5-7 responses were recorded in each tuning direction.

Acknowledgments: Funding for this research was provided in part by NSF Industrial Innovation and Partnerships under award 1827578, the Black & Veatch Building a World of Difference Faculty Fellowship to NFR, a 3M Non-tenured Faculty Award to MDB, and Iowa State University startup funds.

Conflict of Interest: None to report.

Keywords: Resonant sensor, kirigami, wireless sensor, deformation, resonant frequency

References

- [1] S. Patel, H. Park, P. Bonato, L. Chan, M. Rodgers, *J. Neuroeng. Rehabil.* **2012**, 9, 21.
- [2] S. Cotin, H. Delingette, N. Ayache, *IEEE Trans. Vis. Comput. Graph.* **1999**, 5, 62.
- [3] S. Kawamura, K. Kanaoka, Y. Nakayama, J. Jeon, D. Fujimoto, in *Robot. Autom.* **2003**.

- 1 *Proceedings. ICRA'03. IEEE Int. Conf.*, IEEE, **2003**, pp. 816–821.
- 2 [4] C. T. Gentile, M. Wallace, T. D. Avalon, S. Goodman, R. Fuller, T. Hall, **1992**.
- 3 [5] P. Gardonio, S. J. Elliott, *J. Sound Vib.* **2005**, 284, 1.
- 4 [6] T. A. Erhart, **1996**.
- 5 [7] F. Lorussi, W. Rocchia, E. P. Scilingo, A. Tognetti, D. De Rossi, *IEEE Sens. J.* **2004**, 4, 807.
- 6 [8] F. Lorussi, E. P. Scilingo, M. Tesconi, A. Tognetti, D. De Rossi, *IEEE Trans. Inf. Technol.*
- 7 *Biomed.* **2005**, 9, 372.
- 8 [9] P.-C. Lin, H. Komsuoglu, D. E. Koditschek, *IEEE Trans. Robot.* **2005**, 21, 411.
- 9 [10] B. Glišić, N. Simon, *Cem. Concr. Compos.* **2000**, 22, 115.
- 10 [11] C. Cochrane, V. Koncar, M. Lewandowski, C. Dufour, *Sensors* **2007**, 7, 473.
- 11 [12] T. Yamada, Y. Hayamizu, Y. Yamamoto, Y. Yomogida, A. Izadi-Najafabadi, D. N. Futaba, K.
- 12 Hata, *Nat. Nanotechnol.* **2011**, 6, 296.
- 13 [13] M. Wehner, R. L. Truby, D. J. Fitzgerald, B. Mosadegh, G. M. Whitesides, J. A. Lewis, R. J.
- 14 Wood, *Nature* **2016**, 536, 451.
- 15 [14] S. Ryu, P. Lee, J. B. Chou, R. Xu, R. Zhao, A. J. Hart, S.-G. Kim, *ACS Nano* **2015**, 9, 5929.
- 16 [15] J. J. Park, W. J. Hyun, S. C. Mun, Y. T. Park, O. O. Park, *ACS Appl. Mater. Interfaces* **2015**,
- 17 7, 6317.
- 18 [16] A. Mohammadi Nasab, A. Sabzehzar, M. Tatari, C. Majidi, W. Shan, *Soft Robot.* **2017**, 00,
- 19 soro. 2016.0039.

- 1 [17] M. D. Bartlett, N. Kazem, M. J. Powell-palm, X. Huang, W. Sun, J. A. Malen, C. Majidi,
2 *Proc. Natl. Acad. Sci.* **2017**, 114, 2143.
- 3 [18] R. F. Shepherd, F. Ilievski, W. Choi, S. a Morin, A. a Stokes, A. D. Mazzeo, X. Chen, M.
4 Wang, G. M. Whitesides, *Proc. Natl. Acad. Sci.* **2011**, 108, 20400.
- 5 [19] W. Shan, T. Lu, C. Majidi, *Smart Mater. Struct.* **2013**, 22, 085005.
- 6 [20] A. M. V. Mohan, N. H. Kim, Y. Gu, A. J. Bandodkar, J. M. You, R. Kumar, J. F. Kurniawan, S.
7 Xu, J. Wang, *Adv. Mater. Technol.* **2017**, 2, 1.
- 8 [21] Y. Jia, K. Sun, F. J. Agosto, M. T. Quiñones, *Meas. Sci. Technol.* **2006**, 17, 2869.
- 9 [22] R. Matsuzaki, A. Todoroki, *Sensors Actuators A Phys.* **2006**, 126, 277.
- 10 [23] J. C. Butler, A. J. Vigliotti, F. W. Verdi, S. M. Walsh, *Sensors Actuators, A Phys.* **2002**, 102,
11 61.
- 12 [24] M. D. Bartlett, E. J. Markvicka, C. Majidi, *Adv. Funct. Mater.* **2016**, 26, 8496.
- 13 [25] J. Zhong, Q. Zhong, Q. Hu, N. Wu, W. Li, B. Wang, B. Hu, J. Zhou, *Adv. Funct. Mater.* **2015**,
14 25, 1798.
- 15 [26] J. T. Muth, D. M. Vogt, R. L. Truby, Y. Mengüç, D. B. Kolesky, R. J. Wood, J. a. Lewis, *Adv.*
16 *Mater.* **2014**, 26, 6307.
- 17 [27] J. Lee, S. Kim, J. Lee, D. Yang, B. C. Park, S. Ryu, I. Park, *Nanoscale* **2014**, 6, 11932.
- 18 [28] V. Savage, C. Chang, B. Hartmann, in *Proc. 26th Annu. ACM Symp. User Interface Softw.*
19 *Technol.*, ACM, **2013**, pp. 447–456.

- 1 [29] R. Mautz, S. Tilch, in *Indoor Position. Indoor Navig. (IPIN), 2011 Int. Conf.*, IEEE, **2011**, pp.
2 1–7.
- 3 [30] H. Bau, N. F. DeRoos, B. Kloeck, W. Göpel, J. Hesse, J. N. Zemel, *Sensors, Mechanical*
4 *Sensors*, Wiley, **2008**.
- 5 [31] T. J. Harpster, B. Stark, K. Najafi, *Sensors Actuators, A Phys.* **2002**, 95, 100.
- 6 [32] K. G. Ong, C. A. Grimes, C. L. Robbins, R. S. Singh, *Sensors Actuators, A Phys.* **2001**, 93, 33.
- 7 [33] N. F. Reuel, J. C. McAuliffe, G. A. Becht, M. Mehdizadeh, J. W. Munos, R. Wang, W. J.
8 Delaney, *ACS Sensors* **2016**, 1, 348.
- 9 [34] J. Zhai, T. V. How, B. Hon, *CIRP Ann. - Manuf. Technol.* **2010**, 59, 187.
- 10 [35] M. Yvanoff, J. Venkataraman, *IEEE Trans. Antennas Propag.* **2009**, 57, 885.
- 11 [36] C. Li, Q. Tan, W. Zhang, S. Member, C. Xue, J. Xiong, **2015**, 15, 1055.
- 12 [37] R. A. Potyrailo, W. G. Morris, **2007**, 79, 45.
- 13 [38] K. G. Ong, J. S. Bitler, C. A. Grimes, L. G. Puckett, L. G. Bachas, *Sensors* **2002**, 2, 219.
- 14 [39] S. Charkhabi, A. Beierle, M. D. McDaniel, N. F. Reuel, *ACS Sensors* **2018**, DOI
15 10.1021/acssensors.8b00267.
- 16 [40] X. Huang, Y. Liu, H. Cheng, W. Shin, J. A. Fan, Z. Liu, C. Lu, G. Kong, K. Chen, D. Patnaik,
17 *Adv. Funct. Mater.* **2014**, 24, 3846.
- 18 [41] S.-Y. Wu, W. Hsu, *Smart Mater. Struct.* **2013**, 22, 105015.
- 19 [42] A. Massarini, M. K. Kazimierczuk, *IEEE Trans. power Electron.* **1997**, 12, 671.

- 1 [43] F. Liu, Y. Chen, H. Song, F. Zhang, Z. Fan, Y. Liu, X. Feng, J. A. Rogers, Y. Huang, Y. Zhang,
2 *Small* **2019**, *15*, 1804055.
- 3 [44] M. Kubo, X. Li, C. Kim, M. Hashimoto, B. J. Wiley, D. Ham, G. M. Whitesides, *Adv. Mater.*
4 **2010**, *22*, 2749.
- 5 [45] J. H. So, J. Thelen, A. Qusba, G. J. Hayes, G. Lazzi, M. D. Dickey, *Adv. Funct. Mater.* **2009**,
6 *19*, 3632.
- 7 [46] S. Cheng, A. Rydberg, K. Hjort, Z. Wu, *Appl. Phys. Lett.* **2009**, *94*, DOI 10.1063/1.3114381.
- 8 [47] L. Teng, K. Pan, M. P. Nemitz, R. Song, Z. Hu, A. A. Stokes, *Soft Robot.* **2018**, *00*, 1.
- 9 [48] Y. H. Chan, Z. Tse, H. Ren, in *Adv. Robot. (ICAR), 2017 18th Int. Conf.*, IEEE, **2017**, pp. 432–
10 437.
- 11 [49] D.-G. Hwang, M. D. Bartlett, *Sci. Rep.* **2018**, *8*, 3378.
- 12 [50] Z. Yan, M. Han, Y. Yang, K. Nan, H. Luan, Y. Luo, Y. Zhang, Y. Huang, J. A. Rogers, *Extrem.*
13 *Mech. Lett.* **2017**, *11*, 96.
- 14 [51] D. G. Hwang, K. Trent, M. D. Bartlett, *ACS Appl. Mater. Interfaces* **2018**, *10*, 6747.
- 15 [52] L. Yin, R. Kumar, A. Karajic, L. Xie, J. M. You, D. Joshua, C. S. Lopez, J. Miller, J. Wang, *Adv.*
16 *Mater. Technol.* **2018**, *3*, 1.
- 17 [53] A. Rafsanjani, Y. Zhang, B. Liu, S. M. Rubinstein, K. Bertoldi, *Sci. Robot.* **2018**, *3*, eaar7555.
- 18 [54] M. A. Dias, M. P. McCarron, D. Rayneau-Kirkhope, P. Z. Hanakata, D. K. Campbell, H. S.
19 Park, D. P. Holmes, *Soft Matter* **2017**, *13*, 9087.

- 1 [55] A. Firouzeh, J. Paik, *IEEE Sens. J.* **2015**, *15*, 6390.
- 2 [56] A. Baldwin, E. Meng, in *Micro Electro Mech. Syst. (MEMS), 2017 IEEE 30th Int. Conf.*, IEEE,
3 **2017**, pp. 227–230.
- 4 [57] R. Sun, B. Zhang, L. Yang, W. Zhang, I. Farrow, F. Scarpa, J. Rossiter, *Appl. Phys. Lett.*
5 **2018**, *112*, 1.
- 6 [58] Z. Yan, T. Pan, G. Yao, F. Liao, Z. Huang, H. Zhang, M. Gao, Y. Zhang, Y. Lin, *Sci. Rep.* **2017**,
7 *7*, 1.
- 8 [59] X. Liu, S. Yao, S. V Georgakopoulos, B. S. Cook, M. M. Tentzeris, in *Microw. Symp. (IMS),*
9 *2014 IEEE MTT-S Int.*, IEEE, **2014**, pp. 1–4.
- 10 [60] S. Yao, X. Liu, S. V. Georgakopoulos, M. M. Tentzeris, *IEEE Antennas Propag. Soc. AP-S Int.*
11 *Symp.* **2014**, *2*, 374.
- 12 [61] H. Fu, K. Nan, W. Bai, W. Huang, K. Bai, L. Lu, C. Zhou, Y. Liu, F. Liu, J. Wang, M. Han, Z.
13 Yan, H. Luan, Y. Zhang, Y. Zhang, J. Zhao, X. Cheng, M. Li, J. W. Lee, Y. Liu, D. Fang, X. Li, Y.
14 Huang, Y. Zhang, J. A. Rogers, *Nat. Mater.* **2018**, *17*, 268.
- 15 [62] S. Yao, S. V Georgakopoulos, B. Cook, M. Tentzeris, in *Microw. Symp. (IMS), 2014 IEEE*
16 *MTT-S Int.*, IEEE, **2014**, pp. 1–4.
- 17 [63] X. Liu, S. Yao, B. S. Cook, M. M. Tentzeris, S. V Georgakopoulos, *IEEE Trans. Antennas*
18 *Propag.* **2015**, *63*, 5897.
- 19 [64] W. Bao, A. K. Mondal, J. Xu, C. Wang, D. Su, G. Wang, *J. Power Sources* **2016**, *325*, 286.

1 [65] L. C. Shen, S. Long, M. Allerdin, M. Walton, *IEEE Trans. Antennas Propag.* **1977**, 25, 595.

2 [66] S. S. Mohan, M. del Mar Hershenson, S. P. Boyd, T. H. Lee, *IEEE J. Solid-State Circuits*

3 **1999**, 34, 1419.

4

5